A&A 488, 597–603 (2008)
DOI: 10.1051/0004-6361:20078557

Astronomy & Astrophysics

Chemical and physical small-scale structure in a pre-stellar core

A. Heithausen[1], C. Böttner[2], and F. Walter[3]

[1] Institut für integrierte Naturwissenschaften, Abteilung Physik, Universität Koblenz-Landau, Universitätsstr. 1, 56070 Koblenz, Germany
e-mail: heithausen@uni-koblenz.de
[2] Radioastronomisches Institut, Universität Bonn, Auf dem Hügel 71, 53121 Bonn, Germany
e-mail: christoph-boettner@gmx.de
[3] Max-Planck-Institut für Astronomie, Königstuhl 17, 69117 Heidelberg, Germany
e-mail: walter@mpia-hd.mpg.de

Received 27 August 2007 / Accepted 9 June 2008

ABSTRACT

Aims. We present a comparative study of several molecular lines and of the dust contiunuum at 1.2mm in a pre-stellar core that is embedded in the Galactic cirrus cloud MCLD123.5+24.9. Previous studies found that the core is gravitationally stable and shows signs of inward motion.
Methods. Using the Owens Valley (OVRO) and Plateau de Bure (PdB) interferometers we obtained high-angular resolution maps of the core in the carbon monosulfide CS ($2 \rightarrow 1$) and the cyanoacetylene HC_3N ($10 \rightarrow 9$) transitions. Together with CS ($5 \rightarrow 4$), $C^{34}S$ ($3 \rightarrow 2$), and bolometer data obtained with the IRAM 30 m telescope, we analyse the excitation conditions and the structural properties of the cloud.
Results. On the one hand, the new CS ($J = 2 \rightarrow 1$) observations reveal significant substructure on a scale of about 7″, i.e., the beam size, corresponding to about 1050 AU at an adopted distance of 150 pc. On the other hand, the interferometric observations in the HC_3N ($J = 10 \rightarrow 9$) transition shows just one single well resolved clump in the inner part of the core. This core is well described by an intensity profile following from a centrally peaked volume density distribution. We find no evidence for depletion of CS onto dust grains. The inward motion seen in the CS ($2 \rightarrow 1$) occurs one-sided from the middle of the filamentary cloud towards the HC_3N core.

Key words. ISM: clouds – ISM: abundances – ISM: molecules – stars: formation

1. Introduction

Dense cores in molecular clouds are the birthplaces of stars. One of the questions of current interest focusses on the evolution from a core to a protostar. Different classifications have been proposed, which are based on different observational diagnostics. Based on the detection or non-detection of IRAS point sources, cores have been separated into stellar or starless cores (Beichman et al. 1986; Benson & Myers 1989). Because this classification is limited by the sensitivity and angular resolution of the IRAS satellite, in recent years some of the cores originally classified as "starless" showed the presence of embedded point sources (e.g., Young et al. 2004).

A different classification scheme was proposed by Ward-Thompson et al. (1994, 1999), who classified cores on the basis of the non-existence or existence of submm point sources as pre-protostellar (later on named "pre-stellar" for brievity, Ward-Thompson et al. 1999) or protostellar. Unlike the classification of a core as being protostellar or stellar, prestellar cores cover a much wider range in their evolutionary states. Not all are necessarily gravitationally bound, while some of them could be in an early stage of contraction. To better quantify their state it is therefore necessary to study more pre-stellar cores in different environments.

We continue our study of dense cores in Galactic cirrus clouds (e.g., Böttner 2005), and concentrate on MCLD123.5+24.9. Based on the above discussed definitions the core is both starless and pre-stellar. Nevertheless, CS observations towards part of the core obtained at high spectral resolution with the IRAM 30 m telescope (Heithausen 1999, hereafter Paper I) revealed double-peaked CS profiles, which are interpreted as signature for infall motion (Myers et al. 1996; Choi et al. 1995). This suggested a scenario of a possibly collapsing fragment embedded in a cloud that is gravitational unbound on larger scales. Further support for this idea was given by dust continuum and HC_3N spectral line observations, which showed that the cloud fragment was indeed gravitionally bound (Heithausen et al. 2002, hereafter Paper II).

The core itself is chemically evolved, showing a large number of molecules with abundances similar to other dense cores with on-going star-formation (Großmann et al. 1990; Großmann & Heithausen 1992; Heithausen et al. 1995; Gerin et al. 1997). Based on NH_3, HCN, HNC, and HCO^+ observations, a low kinetic temperature of less than 15 K was derived and its chemical abundances are well described by low-temperature chemistry with no indication of shock chemistry (Großmann & Heithausen 1992). The low temperature was confirmed with observations of the submm- and far-infrared continuum radiation, which revealed a dust temperature of only 13 K (Bernard et al. 1999). Subsequent observations of SO, CS, CCH, and C_3H_2 confirmed high column densities ($N(H_2) \approx 10^{22}$ cm^{-2}) and volume densities ($n(H_2) \approx 10^5$ cm^{-3}) of the core (Heithausen et al. 1995; Gerin et al. 1997).

At an adopted distance of 150 pc (Heithausen & Thaddeus 1990) the core as seen in the dust continuum at 250 GHz or in $C^{18}O$ emission has a size of 0.18 pc × 0.03 pc (Paper II). On that scale the core shows significant variation of its chemical abundances (Gerin et al. 1997), e.g., cyanoacetylene, HC_3N, was

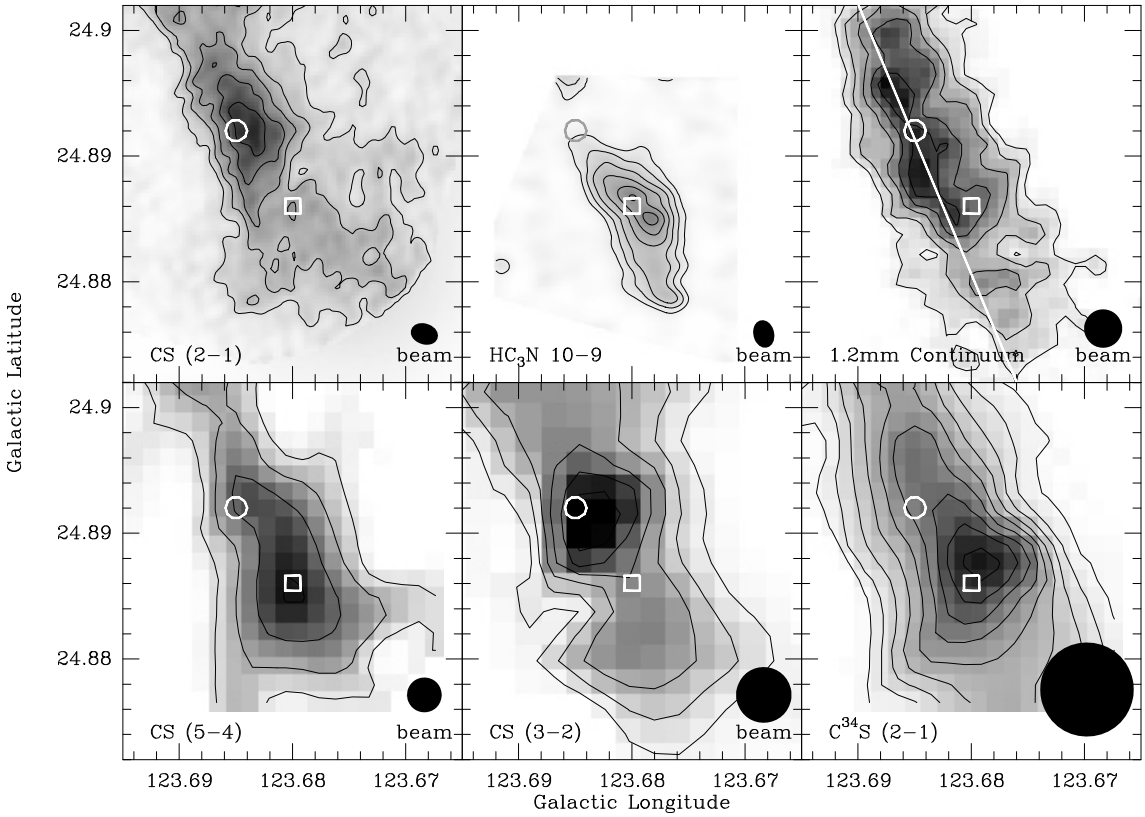

Fig. 1. Comparison of integrated intensity maps in different CS lines with maps in the dust continuum at 1.2 mm and in the HC_3N (10 → 9) line. Beamsizes are indicated in *the lower right corner* of each map. The open square marks the centre position of HC_3N-B, the open circle that of CS-C. Contours are every 0.4 K km s^{-1} starting at 0.8 K km s^{-1} for the CS (2 → 1) line (*top left*); every 0.1 K km s^{-1} starting at 0.2 K km s^{-1} for the HC_3N (10 → 9) line (*top middle*); and every 2 mJy/beam starting at 2 mJy/beam for the dust continuum map (*top right*); every 0.14 K km s^{-1} starting at 0.14 K km s^{-1} for the CS (5 → 4) line (*bottom left*); every 0.25 K km s^{-1} starting at 0.25 K km s^{-1} for the CS (3 → 2) line (*bottom middle*); and every 0.06 K km s^{-1} starting at 0.06 K km s^{-1} for the $C^{34}S$ (2 → 1) line (*bottom right*). The white line in the bolometer map indicates the major axis of the filamentary cloud.

found only at the ends of the filamentary structure, which was interpreted as being caused by different chemical ages of the different regions (Paper II).

All these results so far were obtained with moderate angular resolution of single dish telescopes. With such observations it is difficult to get detailed information on the density structure of the core or to study the connection between the inward motion and the densest region of the core. Therefore, we present the first high-angular resolution data of this core in several spectral lines obtained with the Plateau de Bure (PdB) and the Owens Valley (OVRO) radio interferometers. At the distance of the core we reach an linear resolution of about 1000 AU. Details on the observations are presented in Sect. 2. The results of the observations are discussed in Sect. 3. Implications on the density structure and chemistry of the core are described in Sect. 4. The paper is ended with some conclusions.

2. Observations

The observations of the HC_3N (10 → 9) transition at 90.98 GHz were conducted between May and November 2002 with the IRAM Plateau de Bure (PdB) interferometer. During four runs five antennas in the configuration 5D were used, one run was carried out with 6 antennas in configuration 6Dp. The phase and amplitude were calibrated with frequent observations of the quasars 1928+738 and 0716+714 and the amplitude scale was derived from measurements of MWC349 and CRL618. The velocity resolution was 0.05 km s^{-1} channels.

We also observed MCLD 123.5+24.9 in the CS (2−1) line using the Caltech OVRO millimeter interferometer from January to April 2001. In total, 5 tracks were spent on source (2 pointings each) in the "C" and "L" configurations. The nearby source J1803+784 (1.5 Jy) was used for phase calibration. The velocity resolution was 0.1 km s^{-1}.

Both interferometric data sets consist of single maps centred on CS-C (Paper I, s. Fig. 1) and HC_3N-B (Paper II), respectively. They were corrected for missing zero spacing using low angular resolution data previously obtained with the IRAM 30 m telescope (Papers I and II); for the correction we applied the method described by Weiß et al. (2001). In the CS map a larger fraction of diffuse emission was missing, whereas in the HC_3N line most of the flux was recovered. The effective synthesized beam FWHM of 6″×8″ is identical in both observations however with different position angles of PA = −72° for CS and PA = −13.5° for HC_3N, respectively; it corresponds to 0.0044 pc × 0.0058 pc or 870 AU × 1160 AU at the distance of 150 pc.

The $C^{34}S$ (2 → 1) and CS (5 → 4) observations were observed simultaneously with the IRAM 30 m telescope in September 2000. We mapped the whole cloud on a 15″ grid, which resulted in a total of 82 spectra. The beam size of the telescope was 27″ at 96.4 GHz and 11″ at 244.9 GHz. Spectra were obtained with an autocorrelation spectrometer set to a velocity resolution of 0.06 km s^{-1} at the lower frequency

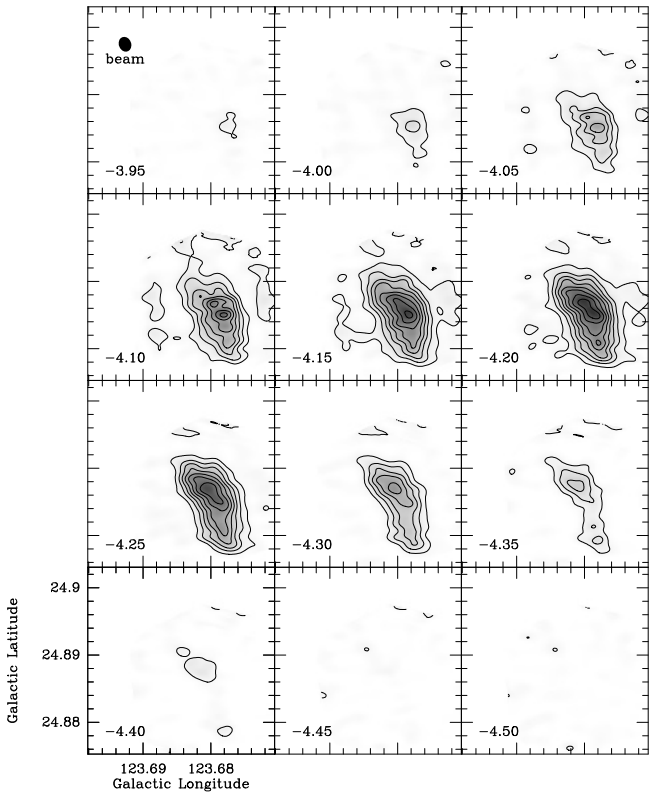

Fig. 2. Channel maps of HC_3N-B in the HC_3N (10→9) line as obtained with the Plateau de Bure interferometer. The beam is indicated in *the top left map*. The centre velocity of each channel (v_{LSR}) is indicated in *the lower left* corner of each map. Contours are every 0.3 K starting at 0.3 K.

and 0.048 km s^{-1} at the higher frequency. Main beam efficiencies η_{mb} of the telescopes at the different frequencies were $\eta_{mb} = 0.82$ at 96 GHz and 0.43 at 245 Ghz. We use the main beam brightness temperature scale T_{mb} for the spectral line data.

For the further analysis, we also use our previously obtained CS (3 → 2) data (Paper I) and 1.2 mm bolometer data (Paper II).

3. Results

3.1. Comparison of the different data sets

A comparison of the appearance of the core in different spectral lines and in the dust continuum is shown in Fig. 1. As was also visible in previous low angular resolution data (see Paper II), the core has a filamentary structure that is most pronounced in the dust map. Taking the different angular resolutions into account all CS maps look similar, however with the location of the maximum shifted from higher Galactic latitudes in the CS (2 → 1) and (3 → 2) maps towards lower latitudes in the CS (5 → 4) and $C^{34}S$ (2 → 1) maps.

The biggest difference in the appearance of the different molecules is between the HC_3N (10 → 9) and the CS (2 → 1) maps: the CS emission is spread over the whole observed region, whereas the HC_3N emision is concentrated in a single clump. The maximum of the integrated intensity of HC_3N (denoted by HC_3N-B in Paper II) is clearly displaced relative to the maximum (denoted by CS-C in Paper I) of the integrated CS (2 → 1) map. It is, however, found at the same position as those in the CS (5 → 4) and $C^{34}S$ (2 → 1) maps.

Figures 2 and 3 give an overview of the velocity structure of the core in the HC_3N (10 → 9) and CS (2 → 1) spectral lines. The HC_3N emission shows a simple single clump, which is well resolved in our map. The emission of the clump shows very little variation from one velocity channel to the next. In contrast to the CS emission (see below) there is no indication for diffuse HC_3N emission.

The CS channel maps show much more structure with several emission maxima and extensive diffuse emission, which is changing its intensity distribution significantly from one channel map to the next. The emission is spread over most of the observed region.

3.2. Quantification of the emission

To derive accurate positions and velocities of the emission throughout the core, we have quantified the emission seen in the CS and HC_3N maps using the GAUSSCLUMP algorithm developed by Stutzki & Güsten (1990) and discussed by Kramer et al. (1998). This algorithm assumes that the emission of the cloud is composed of regions that have a Gaussian-shaped intensity distribution. Starting at the intensity maximum, it fits a single 3-dimensional Gaussian to the intensity distribution, which is then subtracted. This procedure is repeated with the residual intensity until the noise level is reached. In this way, it subsequently fits the whole cloud into Gaussian-shaped emission blobs. The results for each spectral line are summarised in Table 1.

The HC_3N data are separated into two single clumps. Inspection of the channel maps by eye (see Fig. 2) would probably just define the emission as a singular clump with a small bending at its lower latitude side. The computer analysis defines it as two clumps due to the predefined Gaussian form. More than 90% of the emission is concentrated in the clumps.

For comparison with the HC_3N data, we have also used the GAUSSCLUMP algorithm to quantify the CS (5 → 4) data. Due to the undersampled maps (11″ beam and 15″ sampling) only a single clump was fitted, providing us the global properties for this transition. The analysis of the $C^{34}S$ (2 → 1) data also provides a single emission region with the same centre in position and velocity as the CS (5 → 4) line, indicating that both lines have similar excitation conditions. The results show that the HC_3N clumps have no correspondance in neither the $C^{34}S$ (2 → 1) nor the CS (5 → 4) clumps. While the position of the CS clump on the sky is almost coincident with HC_3N position, it is separated in velocity space by at least 0.1 km s^{-1}, which corresponds to about half of the line width of only 0.24 km s^{-1}.

This separation is confirmed by a direct comparison of the spectra of the CS (5 → 4), $C^{34}S$ (2 → 1), and the HC_3N (10 → 9) lines from the IRAM 30 m telescope at the position of the HC_3N maximum (Fig. 6). The Gaussian fit to the spectra provides identical centre velocities for both CS lines at $v_{LSR} = -4.11 \pm 0.01$ km s^{-1}, and identical line widths of $\Delta v = 0.33 \pm 0.03$ km s^{-1}, compared to the HC_3N line centred at $v_{LSR} = -4.19 \pm 0.01$ km s^{-1}, and a much narrower line width of $\Delta v = 0.22 \pm 0.02$ km s^{-1}.

For a comparison with the other presumably optically thin lines, we have also separated the CS (2 → 1) emission into Gaussian-shaped regions. We are aware that this line is optically thick (see Sect. 4.3) and that therefore the identification of these Gaussian-shaped emission regions with physical substructure in the cloud is not necessarily admissible. We list however these parameters from our fit, to allow for a better quantitative comparison with the other spectral lines. The CS (2 → 1) data are separated into at least 5 individual Gaussian regions, which account for about half of the total emission, indicating again that

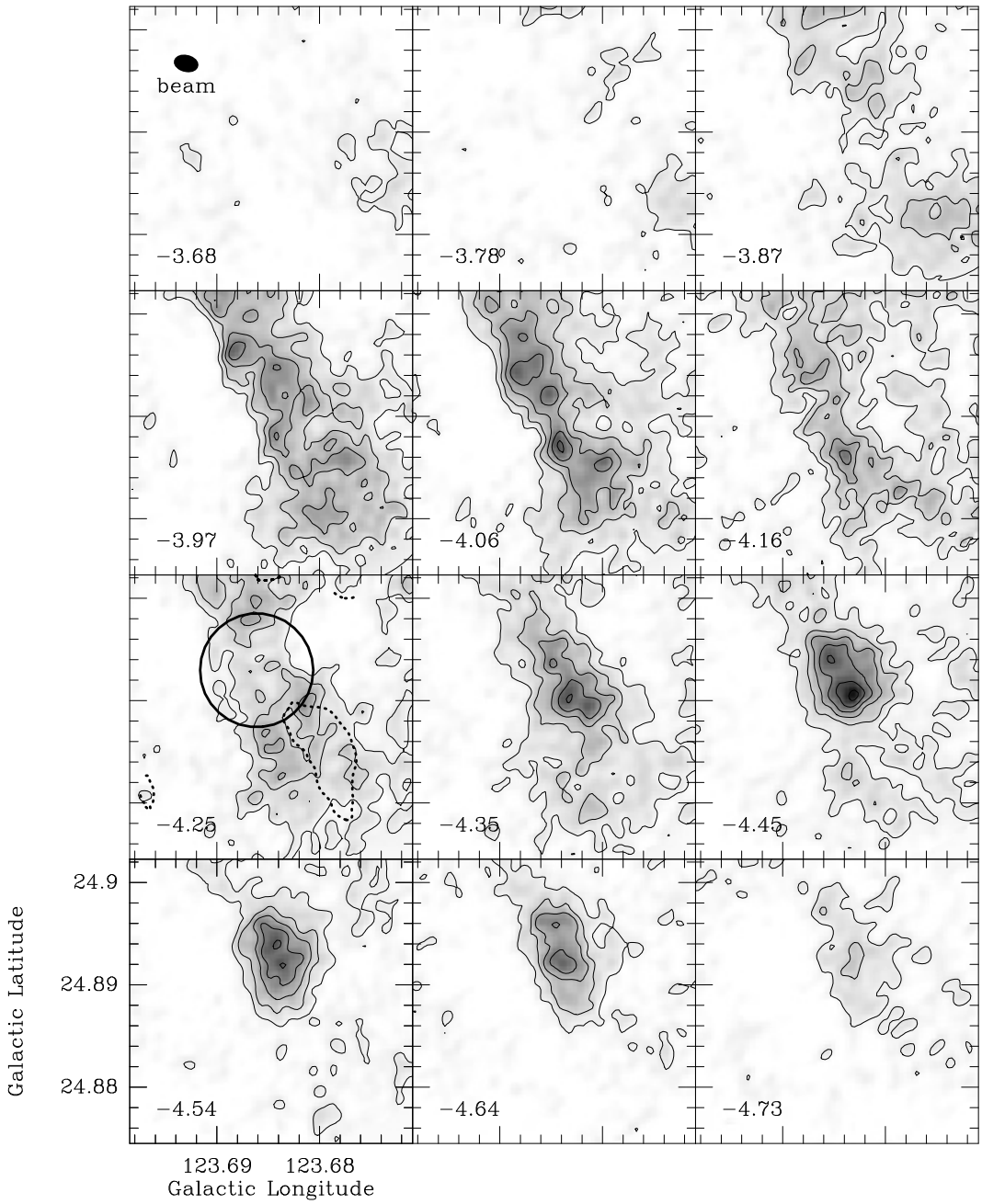

Fig. 3. Channel maps of CS-C in the CS (2→1) line as obtained with the OVRO interferometer. The centre velocity of each channel ($v_{\rm LSR}$) is indicated in the lower left corner of each map. Note that the step between two channelmaps is larger than in the HC_3N maps (see Fig. 2). The beam is indicated in the top left map. Contours are every 0.75 K starting at 0.75 K. The black circle in the map at −4.25 km s^{-1} marks the region of self-absorption and the dashed contour indicates the position and size of the HC_3N core.

a significant fraction of the CS gas is in a wider spread diffuse component. The maxima of the most intense ($T_{\rm mb}$) CS (2 → 1) and HC_3N clumps are separated by about 25″. This analysis also confirms that there is no emission line centred at the velocity range of the HC_3N line. A direct comparison of velocity-position cuts through our high angular resolution data cubes illustrates this finding (see Figs. 4 and 5).

3.3. Comparison of HC_3N emission and the infall signature

The southern most part of the core, CS-C, in MCLD123.5+24.9 has been found to show asymmetric self-absorbed CS(2 → 1) and (3 → 2) profiles with the blue shifted part brighter than the red shifted (Paper I). The velocity of the (5 → 4) line was coincident with the absorption dip in the lower transitions. These features are the well tested diagnostics of inward motion in molecular clouds (Zhou et al. 1992; Walker et al. 1994; Myers et al. 1996).

With our new high-angular resolution data, we are able to study in more detail the region where the infall signature occurs. The absorption dip can be easily seen in the channel maps presented in Fig. 3 in the channel at $v_{\rm LSR} = -4.25$ km s^{-1}. Its position is coincident with the intense CS emission seen in these maps from the channel at $v_{\rm LSR} = -4.45$ km s^{-1} downwards (at $l \approx 123\overset{\circ}{.}685, b \approx 24\overset{\circ}{.}892$). In Fig. 3, the location of the double-peaked CS (2 → 1) profiles and that of HC_3N-B are marked.

Table 1. Parameters for the HC_3N and CS emission identified with GAUSSCLUMP.

No.	l (deg)	b (deg)	T_{mb} (K)	v_{lsr} (km s^{-1})	Δv (km s^{-1})	$\Delta x \times \Delta y$ ($''\times''$)
			HC_3N (10 → 9)			
#1	123.679	24.885	2.67	–4.19	0.23	17.4 × 33.2
#2	123.683	24.888	0.90	–4.25	0.24	8.1 × 13.0
			CS (5 → 4)			
#1	123.680	24.886	1.3	–4.09	0.36	19 × 44
			$C^{34}S$ (2 → 1)			
#1	123.680	24.888	1.4	–4.10	0.30	30 × 107
			CS (2 → 1)			
#1	123.684	24.890	4.81	–4.44	0.34	16.7 × 35.9
#2	123.688	24.894	3.70	–4.07	0.17	13.2 × 83.7
#3	123.685	24.895	2.45	–3.97	0.21	10.2 × 23.5
#4	123.675	24.881	2.20	–3.97	0.39	14.1 × 31.4
#5	123.682	24.879	2.02	–4.35	0.18	30.7 × 17.3

Remark: data are not corrected for finite resolution.

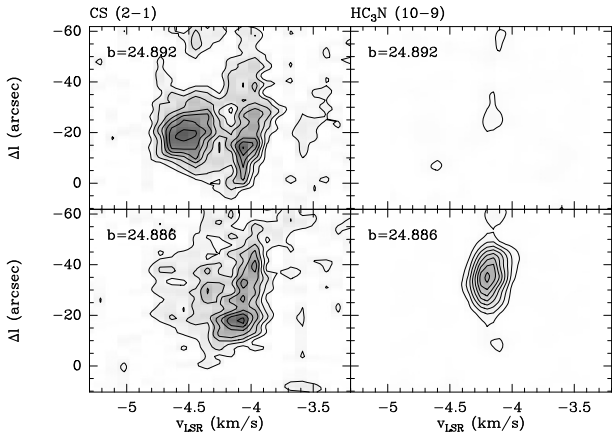

Fig. 4. Velocity-longitude maps of our high-angular resolution CS (2 → 1) (*left maps*) and HC_3N (10 → 9) (*right maps*) data at the location of the HC_3N maximum (*lower map*) and of the CS (2 → 1) maximum (*upper map*). The Galactic latitudes of the cuts are indicated at *the upper left corner*. Contours are every 0.5 K starting at 0.5 K for the CS data, and 0.3 K starting at 0.3 K for the HC_3N data. Offsets in Galactic longitude are relative to l = 123.°689.

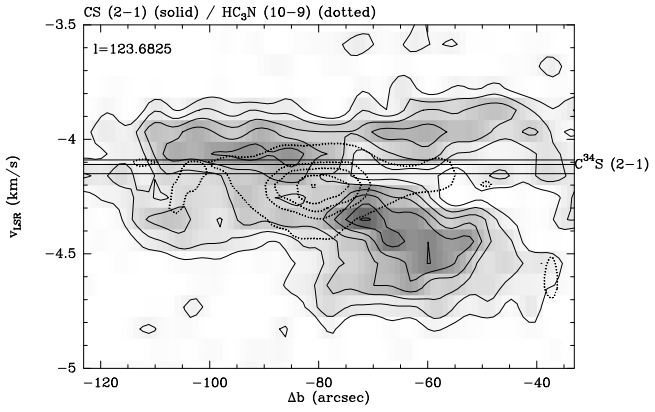

Fig. 5. Velocity-latitude map of our high-angular resolution CS (2 → 1) (solid contours) and HC_3N (10 → 9) (dotted contours) data along the Galactic longitude l = 123.°6825. Contours are every 0.5 K starting at 0.5 K for the CS data and 0.3 K starting at 0.3 K for the HC_3N data. Offsets in Galactic latitude are relative to b = 24.°909. The solid line at v_{LSR} = −4.11 km s^{-1} marks the velocity of the CS (5 → 4) and $C^{34}S$ (2 → 1) lines; *the upper and lower* lines parallel to this line indicate the variation of the centre velocities for these molecules along this cut.

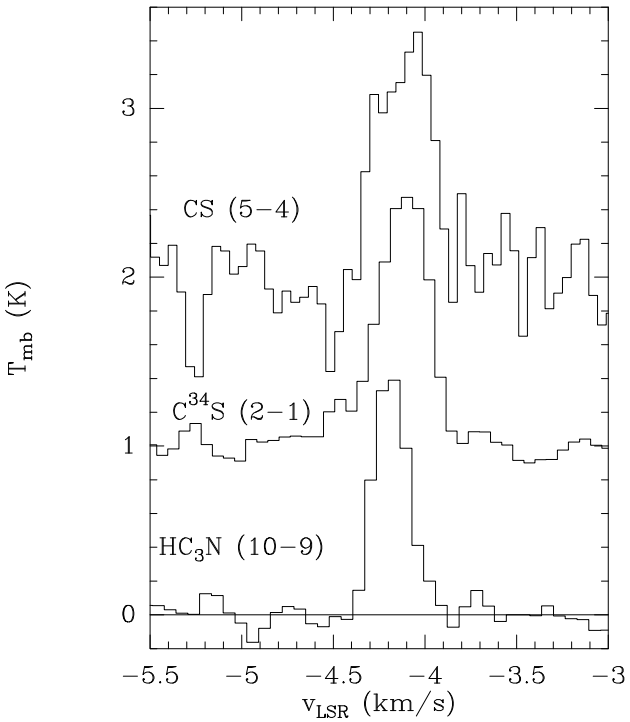

Fig. 6. Comparison of the CS (5 → 4), $C^{34}S$ (2 → 1), and the HC_3N (10 → 9) spectra from the IRAM 30 m telescope at the position of the HC_3N maximum (l = 123.°680, b = 24.°886). For better display the upper spectra have been shifted by 1 K and 2 K, respectively.

Position-velocity maps of this region are shown in Figs. 4 and 5. The infall signature is positionally adjacent, but not coincident with HC_3N-B. Possible explanations for this displacement will be discussed in Sect. 4.3.

4. Discussion

4.1. Intensity and density profile of the dust filament

In Fig. 7, we present an intensity profile of the dust filament seen in Fig. 1. The major axis of this filament has a position angle of 23°. We derived the profile by averaging the intensity along the major axis as function of the minor axis. The intensity distribution is well described by a Gaussian profile with a full-width at half-maximum of 28″. An intensity profile that follows from a constant volume density assuming optically thin continuum emission does not represent the observed data as well. A more detailed analysis of the profile is hampered by the observing technique with which the bolometer data were observed. Due to the chopping secondary mirror with a chop-throw of 50″ to 70″, extended emission on that scale is missing and thus the profile on that scale is unreliable.

4.2. Density profile of the HC_3N core

To determine the intensity profile of HC_3N-B we present the circular average of the intensity distribution centred on HC_3N-B of the integrated (10 → 9) line from Fig. 1. Based on the ratios of the hyperfine components of the lower HC_3N spectral lines we have found in Paper II that these lines have low optical depths. We derived a volume density of about $n_{H_2} \approx 3 \times 10^5$ cm^{-3}. We therefore adopt here also optically thin emission in the (10 → 9) line, i.e., the observed intensity is proportional to the column density. In Fig. 8, we present the results of our profile analysis.

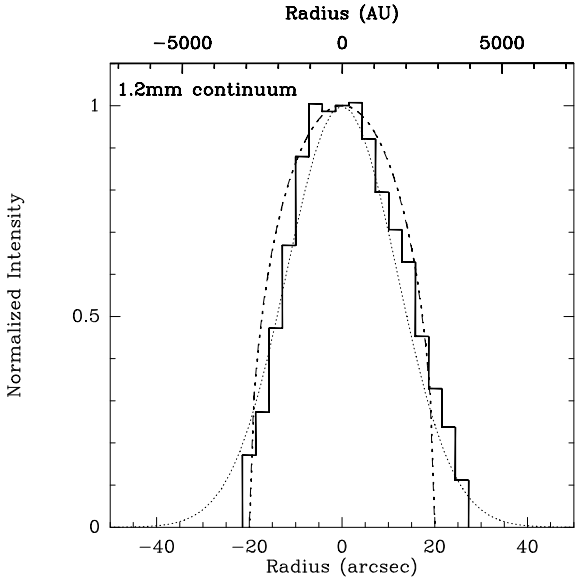

Fig. 7. Density profile along the minor axis of the dust filament (solid line) derived by averaging the intensity along the major axis of the filament. The dotted line represents a Gaussian intensity distribution with a full-width at half-maximum of 28″. The dot-dashed line corresponds to a cylinder seen edge-on with constant volume density and a radius of 20″. The upper scale gives the radius in AU, which is derived by adopting a distance of 150 pc to the cloud.

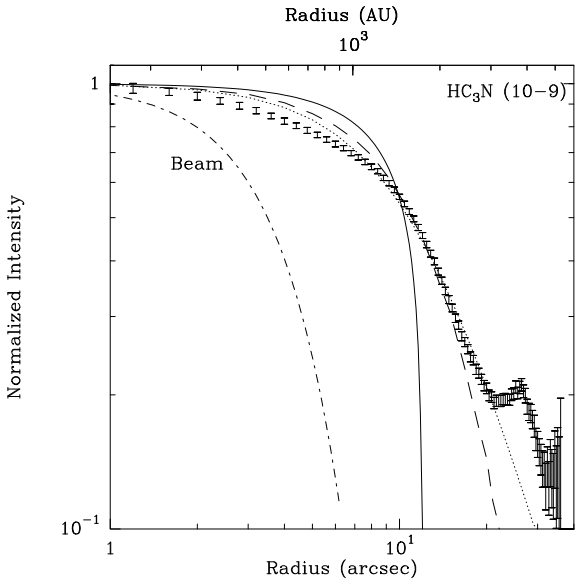

Fig. 8. Density profile of HC_3N-B in the HC_3N (10 → 9) line (error bars). The dot-dashed line corresponds to a beam of 7″, which is the averaged value of the elliptical synthezied beam (6″ × 8″). The long-dashed line represents a Gaussian intensity distribution with full-widths at half-maximum of 17″ × 33″ corresponding to the values listed in Table 1. The solid line shows the intensity profile for an optically thin sphere with constant volume density and a radius of 12″. The dotted line corresponds to a column density profile according to Eq. (1) with $\alpha = 1.2$ and $r_0 = 12.''1$. The upper scale gives the radius in AU.

For comparison with the observed data, we also present some theoretical profiles:

- the intensity profile of a 2-dimensional structure described by two Gaussian profiles with full-width at half-maxima of 17″ × 33″ corresponding to the values listed in Table 1.
- a sphere with constant volume density and a diameter of 24″, corresponding to the geometric mean of the full-widths at half-maximum derived from the GAUSSCLUMP analysis (see Table 1).
- and an intensity profile following

$$I(r) = \frac{I_0}{(1 + r^2/r_0^2)^\alpha} \quad (1)$$

(cf. Johnstone et al. 2003). Assuming optically thin emission, i.e., $I \propto N$, we have varied the projected radius r_0 and the exponent α over wide ranges and found a best solution for $\alpha = 1.2 \pm 0.2$ and $r_0 = 12.''1 \pm 0.''8$, corresponding to 1760 AU at the distance of the cloud.

It is obvious that the profile which assumes a constant density throughout the core does not fit the data well. Density distributions with a centrally peaked density represent the observed intensity distribution much better. The Gaussian intensity distribution, which follows from a Gaussian density distribution, has a gradient that is too flat in the inner part and a too steep gradient at the out part of the core. The column density distribution following Eq. (1) is the best representation of the observed profile.

4.3. The displacement between CS and HC_3N

The displacement between CS-C as seen in the CS (2 → 1) line and HC_3N-B in our high-angular resolution data is striking; it is now much better visible than in our lower angular resolution data (Paper II). It occurs both in the plane of the sky (see Fig. 1) and in velocity (Figs. 4 and 5). We first discuss the possibility of depletion as a cause for the displacement before we discuss the velocity field and its implications on infall motion.

4.3.1. Depletion

Displacements between CS and an other molecules, as, e.g., N_2H^+, has been seen towards other prestellar dense cores (e.g., Lada et al. 2003; Tafalla et al. 2002, 2004). For the prototypical prestellar core B68 it has been interpreted as being caused by depletion of CS onto dust grains (e.g., Tafalla et al. 2002; Di Francesco et al. 2003). To study whether the explanation, that the displacement is caused by depletion, holds also for the core under consideration, we analyse first the optical depth of the CS (2→1) line. The isotopic ratio of $C^{32}S/C^{34}S$ in the interstellar medium equals the solar value of 22.7 (Lucas & Liszt 1998). Therefore, the intensity ratios should be equal to that number if both lines are optically thin. The line averaged ratios, we derive from our observations, are however 6 ± 2 towards the region with inward motion, corresponding to $\tau_{2\to1} = 4 \pm 1$, and 2.5 ± 0.5 towards the HC_3N peak, corresponding to $\tau_{2\to1} \geq 10$. This means that the CS (2 → 1) lines of both regions have high optical depths, with an higher value towards the HC_3N core. The CS (2→1) line is thus not a good tracer for the column density.

There is a much closer agreement between the intensity distributions of the presumably optically thin transitions of CS (5 → 4) and $C^{34}S$ (2 → 1) and the HC_3N (10 → 9) line (see Fig. 1). This suggests that depletion of CS onto dust grains does not play a large role for the different distributions. This is confirmed by the comparison with our bolometer data: within the limits of the different angular resolutions there is also a better aggreement between the optically thin CS(5 → 4) and $C^{34}S$ lines and the dust emission than between dust and the CS (2 → 1) line (see Fig. 1).

4.3.2. Infall motion

The velocity displacement is obvious in our Gaussian analyis of the emission. To illustrate this separation we show in Fig. 4 two longitude-velocity maps obtained at different Galactic latitudes through the core. At the maximum of the CS (2 → 1) line there is almost no corresponding HC_3N emission. At this latitude, the self-absorption of the CS line is most pronounced. Compared to the HC_3N line the maximum of the CS line is clearly blue shifted. The second position-velocity cut is at the latitude of the HC_3N maximum. At the velocity range of the HC_3N line there is only weak CS emission; the CS profile is assymmetric and the CS maximum is clearly red shifted compared to the HC_3N line.

A latitude-velocity map presented in Fig. 5 also illustrates these findings. Double-peaked CS profiles are only found towards the maximum of the CS (2→1) intensity distribution. This region is located at the northern part of HC_3N-B, which indicates the densest part of the core. Towards the lower latitude side of the HC_3N core, the double-peaked CS lines profiles disappear; only a single peaked asymmetric profile at redshifted velocities is seen with a broad wing towards the blue side. In this figure, we also mark the velocity range for the CS (5 → 4) and $C^{34}S$ (2 → 1) lines, which are clearly redshifted throughout the whole region compared to the HC_3N line.

Double-peaked velocity profiles with the blue component stronger than the red one are interpreted as being caused by infall motion (Walkers et al. 1994; Choi et al. 1995; Myers et al. 1996). Such profiles arise from centrally condensed collapsing clouds for spectral lines for which the excitation temperature drops from the core to the outer regions. The formation of such line profiles is nicely illustrated by Walker et al. (1994) in their Fig. 1. The near side of the cloud is receeding from the observer, thus redshifted, while the far side is approaching, thus blueshifted. Due to the gravitational acceleration by the central core the gas closer to the core has higher velocities. Therefore, for the redshifted component, the gas with the lower excitation temperature and the apropriate velocity is between the core and the observer and thus, if optically thick, can absorb. For the approaching component the gas with the proper velocity and a lower excitation temperature is behind the aproaching component and therefore cannot absorb. For spectral lines with higher optical depth this leads to the assymetric spectral line profile with a stronger blue than red component. The velocity of optical thin lines should coincide with the absorption dip.

The profiles we observe for the upper part of the HC_3N core fit this description well (see Fig. 5). The velocity of the HC_3N coincides with the CS absorption dip. The blueshifted component of the CS (2 → 1) line is stronger than the redshifted. We therefore conclude that the upper part of the core is indeed contracting.

At the southern or lower part of the core the situation is more complicated: here the profile reverses; the blueshifted component almost vanishes and thus the redshifted line is the strongest component. We note here that the relation between the redshifted CS component and the HC_3N core does not change much from the upper to the lower part of the core; only the velocity separation between the CS and HC_3N lines decreases. Such a line reversal has been seen towards other cores, e.g., towards L1544 (Tafalla et al. 1998). One explanation for the reversal is that it is a sign for outward motion (Walker et al. 1994). If we adopt this explanation and compare the intensities of the CS lines in the upper and in the lower part of the core we find that there is more material moving inwards to the core than outwards from the core.

5. Conclusions

We presented a high-angular resolution study of the pre-stellar core in MCLD123.5+24.9 in several CS transitions and in the HC_3N (10 → 9) line as well as in the dust continuum. Our observations sharpens the picture of gravitational collapse in that core. The major results of our study are the following:

- the CS emission shows structure down to the smallest scale oberved;
- the HC_3N emission comes from a single well resolved core;
- based on an analysis of the intensity profiles in the dust continuum and in the HC_3N line we find that the core is centrally condensed;
- towards the upper half of the HC_3N core we have clear signs of inward motion;
- towards the lower half the CS profiles could be interpreted as outward motion.

The interpretation of the spectral line profiles follows the standard line discussed in the literature for pre-stellar cores. Other possibilities for the interpretation may exist. Clearly, a radiative transfer modelling is demanded to support or discard this interpretation.

Acknowledgements. C.B. acknowledged financial support from the German Max Planck Society through the International Max Planck Research School (IMPRS). We thank Carsten Kramer for critically reading the manuscript. This work was partly supported by the Deutsche Forschungsgemeinschaft grant SFB-494-C2 and is based on observations carried out with OVRO and the IRAM telescopes; IRAM is supported by INSU/CNRS (France), MPG (Germany) and IGN (Spain).

References

Beichman, C. A., Myers, P. C., Emerson, J. P., et al. 1986, ApJ, 307, 337
Benson, P. J., & Myers, P. C. 1989, ApJS, 71, 89
Bernard, J. P., Abergel, A., Ristorcelli, I., et al. 1999, A&A, 347, 640
Böttner, C. 2005, Ph.D. Thesis, University Bonn
Choi, M., Evans, N. J. II., Gregersen, E. M., & Wang, Y. 1995, ApJ, 448, 742
Di Francesco, J., Hogerheijde, M. R., Welch, W. J., & Bergin, E. A. 2003, AJ, 124, 2749
Gerin, M., Falgarone, E., Joulain, K., et al. 1997, A&A, 318, 579
Großmann, V., & Heithausen, A. 1992, A&A, 264, 195
Großmann, V., Heithausen, A., Meyerdierks, H., & Mebold, U. 1990, A&A, 240, 400
Heithausen, A. 1999, A&A, 345, L53 (Paper I)
Heithausen, A., & Thaddeus, P. 1990, ApJ, 353, L49
Heithausen, A., Corneliussen, U., & Großmann, V. 1995, A&A, 301, 941
Heithausen, A., Bertoldi, F., & Bensch, F. 2002, A&A, 383, 591 (Paper II)
Johnstone, D., Fiege, J. D., Redman, R. O., Feldman, P. A., & Carey, S. J. 2003 ApJ, 588, L37
Kramer, C., Stutzki, J., Röhrig, R., & Corneliussen, U. 1998, A&A, 329, 429
Lada, J., Bergin, E. A., Alves, J. F., & Huard, T. L. 2003, ApJ, 586, 286
Lucas, R., & Liszt, H. 1998, A&A, 337, 246
Myers, P. C., Mardones, D., Tafalla, M., Williams, J. P., & Wilner, D. J. 1996, ApJ, 465, L133
Stutzki, J., & Güsten, R. 1990, ApJ, 356, 513
Tafalla, M., Mardones, D., Myers, P. C., et al. 1998, ApJ, 504, 900
Tafalla, M., Myers, P. C., Caselli, P., Walmsley, C. M., & Comito, C. 2002, ApJ, 569, 815
Tafalla, M., Myers, P. C., Caselli, P., & Walmsley, C. M. 2004, A&A, 416, 191
Walker, C. K., Narayanan, G., & Boss, A. P. 1994, ApJ, 431, 767
Ward-Thompson, D., Scott, P. F., Hills, R. E., & André, P. 1994, MNRAS, 268, 276
Ward-Thompson, D., Motte, F., & André, P. 1999, MNRAS, 305, 143
Weiß, A., Neininger, N., Hüttemeister, S., & Klein, U. 2001, A&A, 365, 571
Young, C. H., Jørgensen, J. K., Shirley, Y. L., et al. 2004, ApJS, 154, 396
Zhou S. 1992, ApJ, 394, 204